

Rapid 3D imaging with an undersampled shells k-space trajectory

Y. Shu¹, S. J. Riederer¹, M. A. Bernstein¹

¹Department of Radiology, Mayo Clinic College of Medicine, Rochester, MN, United States

Introduction

The time required to fully sample 3D Cartesian k-space is relatively long. Alternative non-Cartesian 3D trajectories (1, 2) provide faster coverage of k-space than conventional Fourier sampling. When very fast volume coverage is required, undersampling strategies have been used in conjunction with these non-Cartesian trajectories to further reduce the scan time (3, 4, 5). The purpose of this work is to examine how k-space undersampling by removing interleaves on some shells can be used with the shells trajectory (6).

The shells trajectory (Fig. 1a) is a non-Cartesian 3D k-space acquisition method. It samples k-space data on the surfaces of a series of concentric spherical shells. For each shell, interleaved helical spirals sweep over the surface of the shell from one pole to the other. Because the number of interleaves can vary on a per-shell basis, there is flexibility for controlling the sampling density as a function of the k-space radius.

Methods

Several possibilities to implement the undersampling were studied, including removing shells, removing data points in some readouts, and removing interleaves for some of the shells. Among them, removing interleaves within each shell (Fig. 1b) is a simple and promising way to design the undersampling scheme. A systematic way to determine how many interleaves to remove in a given shell is to vary the sampling density according to a monotonically decreasing curve. We chose the second half of a fixed length Kaiser window. The Kaiser window $w(n)$ is based on zero-order modified Bessel function of the first kind I_0 , can be expressed by:

$$w(n) = I_0 \left[\beta \sqrt{1 - (1 - 2(N + n)/2N)^2} \right] / I_0(\beta),$$

where N is the number of shells and the shell index $n = 1, \dots, N$. The parameter β determines the shape of the window and the degree of tapering. Four different β values were considered (Fig. 2). When undersampling was used, the number of interleaves for each shell $M_{us}(n)$ was calculated by

$$M_{us}(n) = \text{round} \left[M_{fs}(n) w(n) \right],$$

where $M_{fs}(n)$ was the number of interleaves required to satisfy the Nyquist criterion.

All the studies were acquired on a 1.5T GE Signa Horizon LX scanner. In all the experiments, data were acquired on the scanner and saved for offline reconstruction with 3D gridding. A phantom experiment was performed to test the properties of various undersampled shells trajectories. A static phantom with a resolution inset was used. The raw data were obtained with the shells trajectory, and interleaves were selectively discarded to generate the undersampled raw data sets. To compare undersampled and fully sampled acquisitions with equivalent scan time, the same raw data set was re-used, but with outer shells discarded. Head images were also acquired from a healthy human volunteer using the shells trajectory. The imaging parameters are: FOV = 25.6 × 25.6 × 25.6 cm³, image resolution 1.42 × 1.42 × 1.42 mm³, TR = 15ms (phantom) or 25ms (including a CHESS fat saturation pulse for the human study), FA = 20°, readout length = 8.192 ms with 1024 data complex points, receiver BW = ±62.5 kHz (694Hz/pixel). The number of shells = 90, and the (fully-sampled) scan time = 55s (or 95s with fat saturation).

Results

The phantom experiment results are shown in Fig. 3. Coronal images from the 3D data sets are shown for four sampling schemes. The undersampling artifacts are clearly visible in the uniform region of the phantom in data set with $\beta=4.2$. However, the artifacts are not as pronounced in the other undersampled cases with lower β values. When we compare the undersampled data (left) with its fully sampled counterpart (right) at same acquisition time, the spatial resolution is consistently better for the undersampled cases. This is expected because the maximal extent in k-space is greater for an equivalent acquisition time with the shells trajectory when undersampling is used.

Table 1 lists the value of β and the corresponding shots required for the sampling schemes. The relative time required for the acquisition is also listed. Note only 50% of the total scan time required for the fully sampled case is needed for the undersampled acquisition with $\beta=3.2$. To measure the SNR, a small region of interest placed in the homogeneous area of the phantom is used. The SNR values were also normalized through dividing by the square root of scan time, which is listed in last row of Table 1. The decrease in normalized SNR is probably acceptable with $\beta=2$ and 3.2.

Figure 4 shows examples of axially reformatted slices from the 3D image set obtained in the volunteer experiment. The image quality is preserved fairly well with undersampling. Undersampling artifacts manifest only as slight signal variations across the images.

Discussion

The shells trajectory is a 3D non-Cartesian data acquisition method with improved efficiency compared to Cartesian trajectory. It also has favorable self-navigating motion correction properties (6). This work demonstrates that undersampling scheme can be combined with the spherical shells k-space trajectory to further accelerate the acquisition for time-constrained applications. Up to two-fold acceleration can be achieved yielding reasonable image quality with comparable spatial resolution, and only minor artifacts.

References

1. Irarrazabal P, et al. MRM 1995;33:656-662.
2. Thedens DR, et al. MRM 1999;41:1170-1179.
3. Barger AV, et al. MRM 2002;48:297-305.
4. Spiniak J, et al. MRM 2005;54:886-892.
5. Lee JH, et al. MRM 2003;50:1276-1285.
6. Shu Y, et al. ISMRM 2005 #2695.

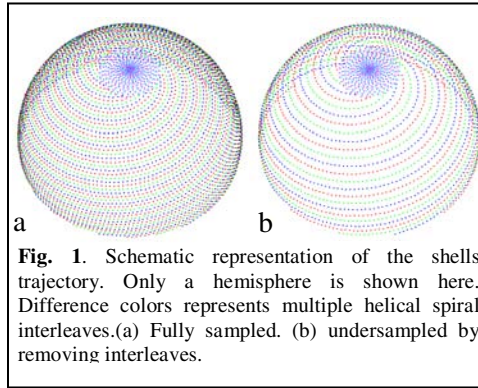


Fig. 1. Schematic representation of the shells trajectory. Only a hemisphere is shown here. Difference colors represents multiple helical spiral interleaves. (a) Fully sampled. (b) undersampled by removing interleaves.

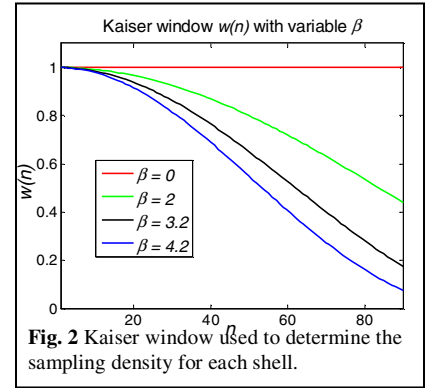


Fig. 2 Kaiser window $w(n)$ used to determine the sampling density for each shell.

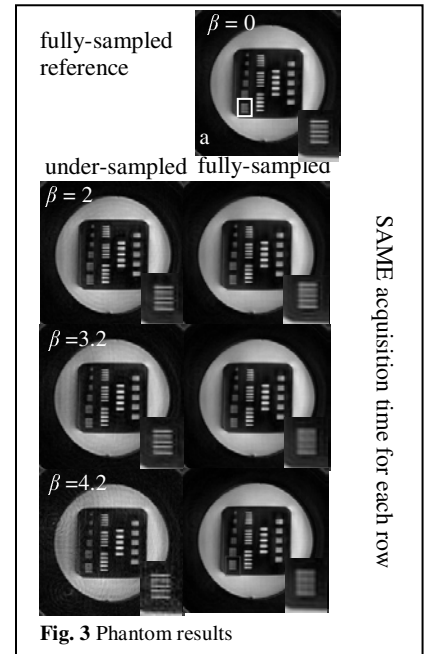


Fig. 3 Phantom results

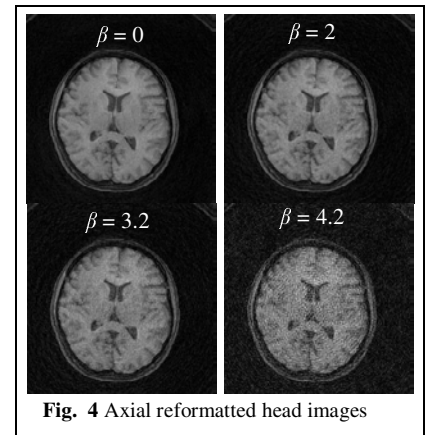


Fig. 4 Axial reformatted head images

Table 1. List of parameters for all the sampling schemes.

β	0	2	3.2	4.2
No. of shots	3595	2480	1808	1456
Relative acq. time	1	0.7	0.5	0.4
SNR	102.9	79.23	60.71	31.21
Normalized SNR	102.9	94.7	85.86	49.36